1   **Supplemental information**

2   **Regulating thermal conductivity of monolayer MnPS$_3$ by magnetic**

3   **phase transition**

4   Dingbo Zhang[1,2§], Ke Wang[3§], Shuai Chen[2], Lifa Zhang[4], Yuxiang Ni[1*], Gang

5   Zhang[2*]

6

7   [1] School of Physical Science and Technology, Southwest Jiaotong University, Chengdu

8   610031, China

9   [2] Institute of High Performance Computing, A*STAR, 138632, Singapore

10   [3] School of Automation, Xi'an University of Posts & Telecommunications, Shaanxi,

11   710121, China

12   [4] NNU-SULI Thermal Energy Research Center, and Center for Quantum Transport

13   and Thermal Energy Science (CQTES), School of Physics and Technology, Nanjing

14   Normal University, Nanjing 210023, China

15

16   §authors contributed equally to this work.

17   *author to whom correspondence should be addressed:

18   yuxiang.ni@swjtu.edu.cn; zhangg@ihpc.a-star.edu.sg

19

20   **Calculation methods**

21   Density functional theory (DFT) [1] calculations are carried out by means of the

22   Vienna ab initio simulation (VASP) package [2] with projector-augmented wave (PAW)

23   potentials [3]. The exchange-correlation functional is treated by using generalized

24   gradient approximation (GGA) with the Perdew-Burke-Ernzerof (PBE) formulation [4].

25   We compute the second-order (harmonic) interatomic force constants (IFCs) using

26   the Phononpy package [5] and the third-order (anharmonic) IFCs using the thirdorder.py

27   code [6]. 3×3×1 supercell was adopted for the calculations of second-order harmonic and

28   third-order anharmonic IFCs, respectively. For the anharmonic IFCs calculations, a

29   cutoff radius (r$_{cutoff}$) of more than 7.0 Å is used. Based on the harmonic and anharmonic

30   IFCs, the lattice thermal conductivity (κ_L) is calculated by solving the phonon

31   Boltzmann transport equation as implemented in the ShengBTE code [7]. For the

32   convergence of thermal conductivity, the phonon sampling k-mesh in the BZ was tested

33   and we adopted a dense phonon q-grid of 40×40×1.

34

1

Lattice constants

2

3 To obtain the experimental lattice constant of $MnPS_3$, we did a comprehensive

4 literature review, and the lattice constants are summarized in Table S1. In Re.[8], the

5 lattice constants of bulk $MnPS_3$ at PM state were measured by neutron diffraction at 90

6 K (a=6.051, b=10.523), slightly smaller than that at AFM state (a=6.077 Å, b=10.524

7 Å)[9,10]. The calculated lattice parameters of bulk $MnPS_3$ are a=6.06~6.183 Å,

8 b=10.406~10.783Å at AFM phases through density functional theory, which agrees

9 well with the experimental results and suggests the validity of DFT calculation on

10 $MnPS_3$.

11 Although substantial studies about 2D $MnPS_3$ have been implemented[11-24], the

12 experimental lattice constants of $MnPS_3$ monolayer are rare. In 2017, Ref.[25]

13 measured the lattice parameters of multi-layer $MnPS_3$ flakes by high-angle annular

14 dark-field (HAADF) HRSTEM image, which are a=6.08±0.05 Å, b=10.52±0.05 Å.

15 These values are close to the experimental lattice constants of bulk $MnPS_3$. In literature,

16 the lattice constants ($a{\neq}b$) are for the conventional cell of $MnPS_3$, but the lattice

17 constant of honeycomb primitive cell (a=b) is always used to describe the geometrical

18 structure of $MnPS_3$ monolayer. For bulk $MnPS_3$, the experimental lattice constant is

19 a=b=6.076 Å for the honeycomb primitive cell as reported in Ref.[26]. In our

20 manuscript, the lattice constants for the primitive cell of $MnPS_3$ monolayer are

21 presented as 6.15, 6.14 and 5.70 Å at AFM, FM, and PM states, respectively. The lattice

22 constant at AFM state is slightly larger than the experimental result of bulk $MnPS_3$ but

23 consistent with the experimental result of 2D $MnPS_3$ flake in Ref.[25] well, while that

24 at FM and PM states agree well with the theoretical results of $MnPS_3$ monolayer in

25 Ref.[27].

26 **Table S1**. Lattice constants for bulk and two-dimensional (2D) $MnPS_3$ at

27 antiferromagnetic (AFM), ferromagnetic (FM), and paramagnetic (PM) states.

System	Lattice constants (Å)	Magnetic state	Reference

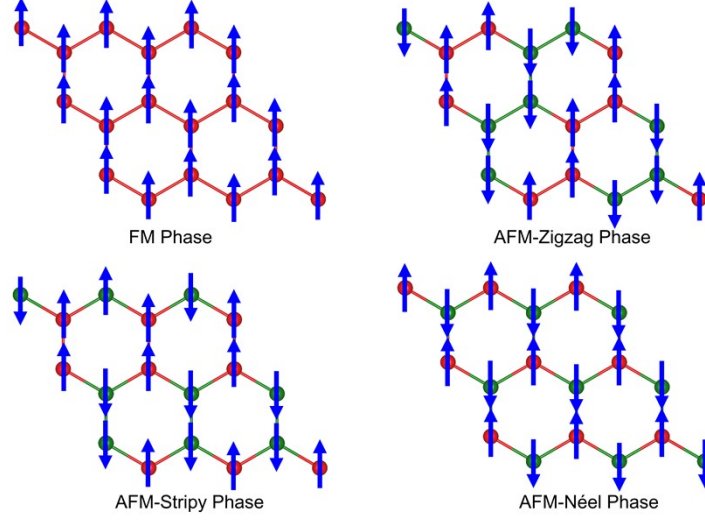|			
Bulk crystal (Exp)	a=6.07, b=10.52	AFM	J. Phys. Soc. Jpn. 52 (11): 3919-3926, 1983
Bulk crystal (Exp)	a=6.051, b=10.523	PM	Phys. Rev. B, 82, 100408(R), 2010
Bulk crystal (Exp)	a=b=5.81	AFM	Adv. Mater. 34, 2200301, 2022
Primitive cell of bulk crystal (Exp)	a=b=6.076	AFM	Comp. Mater. Sci. 177, 109592, 2020
Bulk crystal (DFT/LDA-TS)	a=b=6.235	AFM	
Bulk crystal (DFT/LDA-OBS)	a=b=6.038	AFM	
Bulk crystal (DFT/LDA-Grimme)	a=b=5.995	AFM	
Bulk crystal (DFT)	a=5.93, b=10.36	PM	ACS nano, 10(2): 1738-1743, 2016 (Experimental study)
Bulk crystal (DFT)	a=5.59, 6.06 b=9.98, 10.51	PM, AFM	APL Mater. 7, 081102, 2019 (Experimental study)
Bulk crystal (DFT)	a=6.183, b=10.783	AFM	Appl. Surf. Sci. 543, 148846, 2021
Bulk crystal (DFT)	a=6.008, b=10.406	AFM	Phys. Chem. Chem. Phys. 23, 9679-9685, 2021

Flake (1~6 L) (Exp)	a=6.08±0.05, b=10.524±0.05	AFM	ACS nano, 11(11): 11330-11336, 2017
Monolayer (DFT)	a=5.78, 6.023, 6.00	PM, FM, AFM	Phys. Rev. B, 94, 184428, 2016
Bulk (DFT)	a=5.79, 6.018, 5.99		
Monolayer (DFT)	a=6.06, b=10.498	AFM	J. Mater. Chem. C, 7, 324, 2019 (Experimental study)
Bilayer (DFT)	a=6.06, b=10.495	AFM	
Bulk (DFT)	a=6.067, b=10.509	AFM	
Monolayer (DFT)	a=b=5.88	AFM	Phys. Rev. B, 91, 235425, 2015
Monolayer (DFT)	a=5.69, b=11	PM	Int. J. Hydrogen Energy, 43(11): 5903-5912, 2018.
Monolayer (DFT)	a=6.077, b=10.524	AFM	Nanoscale, 12(45): 23266-23273, 2020 (Experimental study)
Monolayer (DFT)	a=b=6.047	AFM	J. Mater. Chem. C, 8(24): 8098-8106, 2020

1

Magnetic ground state

2

3　　For $MnPS_3$ monolayer with 3×3 supercell, we present four possible magnetic

4 configurations including ferromagnetic (FM), antiferromagnetic-Zigzag (AFM-

5 Zigzag), AFM-Stripy and AFM-Néel in Figure S1, where the non-magnetic P and S

6 atoms are not shown for simplification. To determine the magnetic ground state of

7 $MnPS_3$ monolayer, its total energies at these four magnetic states are calculated, and

8 we found that the energy of FM, AFM- Zigzag and AFM-Stripy states are 197.76,

9 90.29, and 72.78 meV per unit cell higher than AFM-Néel state, respectively, indicating

10 the magnetic ground state of $MnPS_3$ monolayer is AFM-Néel state. This AFM-Néel

1 ground state, where the adjacent magnetic moments on Mn atoms interacted with each

2 other antiparallelly, is consistent with previous theoretical studies[27-30]. Moreover, the

3 AFM ground state in 2D MnPS$_3$ has also been proved experimentally by Raman

4 spectroscopy[13,31], second-harmonic generation[19], and tunneling magnetoresistance[17].

FM Phase   AFM-Zigzag Phase

AFM-Stripy Phase   AFM-Néel Phase

6 **Figure S1**. Possible magnetic configurations of MnPS$_3$ monolayer, including

7 ferromagnetic (FM), antiferromagnetic-Zigzag (AFM- Zigzag), AFM-Stripy and AFM-

8 Néel. The red and green balls represent the spin-up and spin-down Mn atoms.

9 **Phononic properties**

10   The expression for the κ_L, specific heat (C), group velocities (v) and relaxation time

11 of phonon ($\dfrac{1}{\tau^{iso}_\lambda}$) in ShengBTE:

$$\kappa_L = \frac{1}{V}\sum_i C_i \mathrm{v}_i^2 \tau_i^{total}$$

12

$$C_i = \frac{1}{V}\hbar w_i \frac{\partial F_0}{\partial T}$$

13

14 where C_i is the specific heat for phonon mode (i), and F_0 is Bose–Einstein statistics.

$$v_i = \frac{\partial w_i}{\partial k_i}$$

15

$$\frac{1}{\tau^{tol}_\lambda} = \frac{1}{\tau^{ph}_\lambda} + \frac{1}{\tau^{iso}_\lambda} + \frac{1}{\tau^b_\lambda}$$

16

1 where $\dfrac{1}{\tau_i^{ph}}$ is intrinsic anharmonic three-phonon scattering process, $\dfrac{1}{\tau_\lambda^{iso}}$ is the isotope

2 scattering and $\dfrac{1}{\tau_\lambda^{b}}$ is the boundary scattering rate. In our work, the boundary scattering

3 rate is neglected due to its little effect on the thermal conductivity.

$$\frac{1}{\tau_i^{ph}} = \frac{1}{N}\left(\sum_{i'i''}^{+} \Gamma_{ii'i''}^{+} + \sum_{i'i''}^{-} \frac{1}{2}\Gamma_{ii'i''}^{-} + \sum_{i'} \Gamma_{ii'} \right)$$

4

5 $\dfrac{1}{\tau_i^{ph}}$ is the relaxation time of mode i as obtained from perturbation theory. $\Gamma_{ii'i''}^{+}$ and $\Gamma_{ii'i''}^{-}$

6 are three-phonon scattering rates of absorption and emission processes, respectively.

7 They can be expressed as

$$\Gamma_{ii'i''}^{\pm} = \frac{\hbar\pi}{4} \frac{f_0{}' - f_0{}''}{w_i w_{i'} w_{i''}} \left| V_{ii'i''}^{\pm} \right|^2 \delta\left(w_i \pm w_{i'} - w_{i''} \right)$$

8 ,

9 in which the scattering matrix elements $V_{ii'i''}^{\pm}$ are given by

$$V_{ii'i''}^{\pm} = \sum_{a \in u,c} \sum_{b,k} \sum_{\alpha\beta\gamma} \Phi_{abc}^{\alpha\beta\gamma} \frac{e_i^{\alpha}(a) e_{p',\pm q'}^{\beta}(b) e_{p'',\pm q''}^{\gamma}(c)}{\sqrt{M_a M_b M_c}}$$
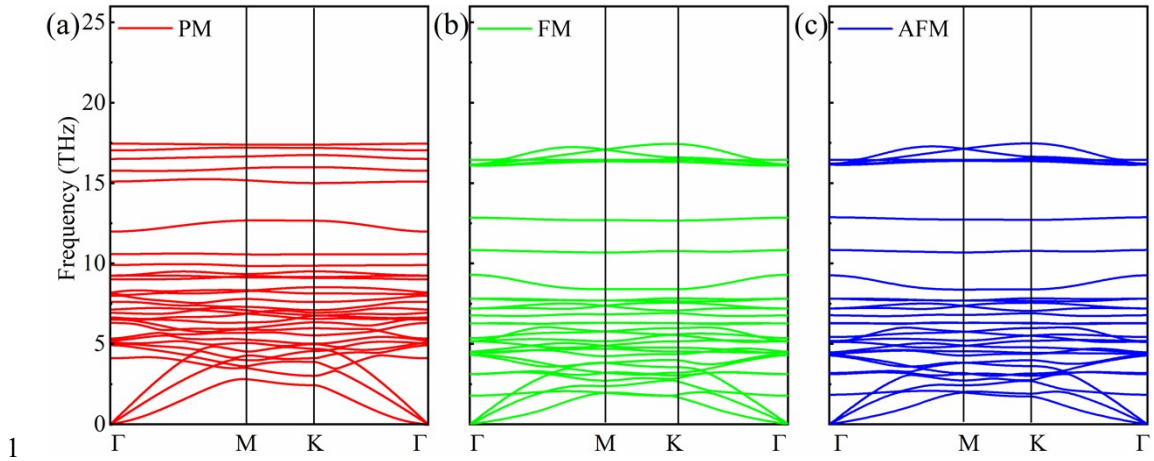
10

11 where for the normalized eigenfunctions $e_{p,q}$ of three phonons involved and on the

$$\Phi_{abc}^{\alpha\beta\gamma} = \frac{\partial^3 E}{\partial r_a^{\alpha} \partial r_b^{\beta} \partial r_c^{\gamma}}$$
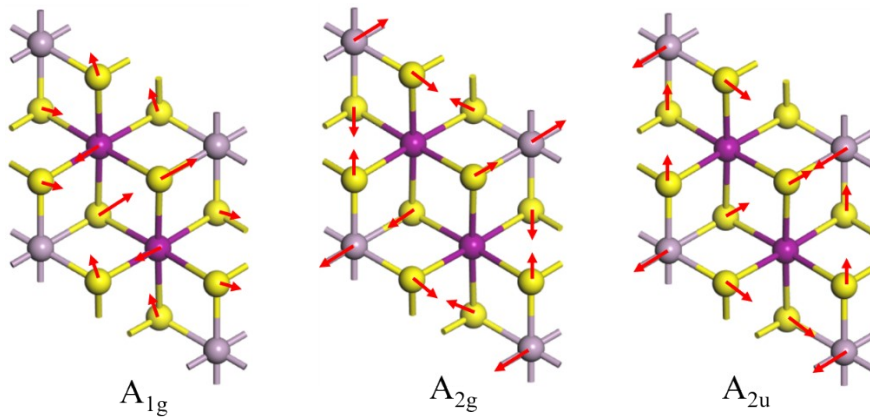
12 anharmonic force constants

13 $\Gamma_{ii'}$ is the contribution to scattering probabilities from isotopic disorder,

$$\Gamma_{ii'} = \frac{\pi w^2}{2} \sum_{a \in u,c} g(a) \left| e_i^{*}(a) \cdot e_{i'}(a) \right|^2 \delta\left(w_i - w_{i'} \right)$$

14

1

2 **Fig. S2.** Phonon dispersions of monolayer $MnPS_3$ with (a) PM, (b) FM and (c) AFM
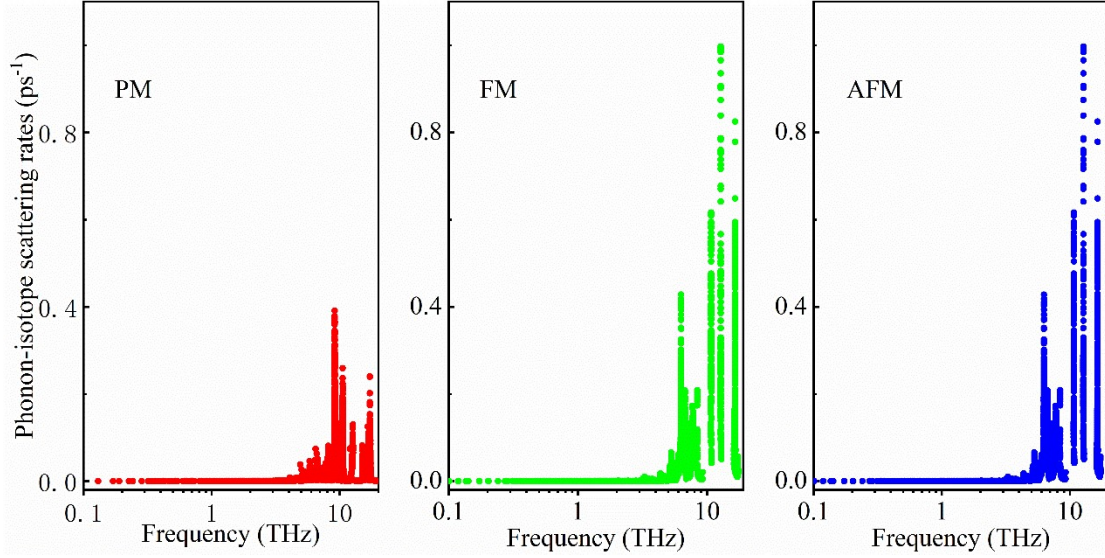
3 phases.

4

5

6 **Fig. S3.** Lattice vibration modes for A_{1g}, A_{2g} and A_{2u}. The red arrow points out the

7 atomic vibration, and the purple, grey and yellow spheres represent Mn, P and S atoms,

8 respectively. A_1g and A_2g are Raman active modes, while A_{2u} is infrared active.

9

10

Fig. S4. The magnetic ordering-dependent phonon-isotope scattering rates.

Table S2. For BAs and MoS$_2$, the calculated thermal conductivity values only considering second- and third-order force constants (FCs), and those including the higher-order force constants, at 200 K.

Thermal conductivity	high-order FCs	only second- and third-order FCs
BAs [Ref. 8]	~ 2500 W/(mK)	~ 2700 W/(mK)
MoS$_2$ [Ref. 9]	~ 200 W/(mK)	~ 200 W/(mK)

Table S3. Maximum group velocities of acoustic phonon modes for monolayer MnPS$_3$ with PM, FM and AFM phases.

maximum group velocity (km/s)	TA	LA
PM	4.62	6.78
FM	4.08	5.84
AFM	3.92	5.62

CIF of paramagnetic MnPS₃

```
data_VESTA_phase_1

_pd_phase_name                      'CIF file                              '
_cell_length_a                      5.70612
_cell_length_b                      5.70612
_cell_length_c                      25.67810
_cell_angle_alpha                   90.00000
_cell_angle_beta                    90.00000
_cell_angle_gamma                    120.00000
_symmetry_space_group_name_H-M       'P 1'
_symmetry_Int_Tables_number          1
loop_
_symmetry_equiv_pos_as_xyz
  'x, y, z'
loop_
  _atom_site_label
  _atom_site_occupancy
  _atom_site_fract_x
  _atom_site_fract_y
  _atom_site_fract_z
  _atom_site_adp_type
  _atom_site_B_iso_or_equiv
  _atom_site_type_symbol
  Mn1    1.0    0.35627    0.64373    0.50000    Biso   1.000   Mn
  Mn2    1.0    0.64373    0.35627    0.50000    Biso   1.000   Mn
  P1     1.0    0.99727    0.99763    0.45813    Biso   1.000   P
  P2     1.0    0.00273    0.00237    0.54187    Biso   1.000   P
  S1     1.0    0.00445    0.65126    0.44201    Biso   1.000   S
  S2     1.0    0.99555    0.34874    0.55799    Biso   1.000   S
  S3     1.0    0.34378    0.34430    0.43892    Biso   1.000   S
  S4     1.0    0.65622    0.65570    0.56108    Biso   1.000   S
  S5     1.0    0.65077    0.00495    0.44201    Biso   1.000   S
  S6     1.0    0.34923    0.99505    0.55799    Biso   1.000   S
```

CIF of ferromagnetic MnPS₃

data_VESTA_phase_1

```
_chemical_name_common                    'CIF file                              '
_cell_length_a                  6.14834
_cell_length_b                  6.14834
_cell_length_c                  22.68656
_cell_angle_alpha               90.00000
_cell_angle_beta                90.00000
_cell_angle_gamma                120.00000
_space_group_name_H-M_alt          'P 1'
_space_group_IT_number             1
loop_
_space_group_symop_operation_xyz
   'x, y, z'
loop_
   _atom_site_label
   _atom_site_occupancy
   _atom_site_fract_x
   _atom_site_fract_y
   _atom_site_fract_z
   _atom_site_adp_type
   _atom_site_B_iso_or_equiv
   _atom_site_type_symbol
   Mn1      1.0    0.333335    0.666667    0.499999    Biso   1.000000 Mn
   Mn2      1.0    0.666665    0.333333    0.500001    Biso   1.000000 Mn
   P1       1.0    0.000995    0.001415    0.451170    Biso   1.000000 P
   P2       1.0    0.999005    0.998585    0.548830    Biso   1.000000 P
   S1       1.0    0.001475    0.681056    0.427426    Biso   1.000000 S
   S2       1.0    0.998525    0.318944    0.572574    Biso   1.000000 S
   S3       1.0    0.322522    0.323145    0.427424    Biso   1.000000 S
   S4       1.0    0.677478    0.676855    0.572576    Biso   1.000000 S
   S5       1.0    0.680434    0.002104    0.427425    Biso   1.000000 S
   S6       1.0    0.319566    0.997896    0.572575    Biso   1.000000 S
```

CIF of antiferromagnetic MnPS$_3$

data_VESTA_phase_1

```
_chemical_name_common                    'CIF file                                    '
_cell_length_a                           6.13782
_cell_length_b                           6.13782
_cell_length_c                           22.76441
_cell_angle_alpha                        90.00000
_cell_angle_beta                         90.00000
_cell_angle_gamma                        120.00000
_space_group_name_H-M_alt                'P 1'
_space_group_IT_number                   1
loop_
_space_group_symop_operation_xyz
   'x, y, z'
loop_
   _atom_site_label
   _atom_site_occupancy
   _atom_site_fract_x
   _atom_site_fract_y
   _atom_site_fract_z
   _atom_site_adp_type
   _atom_site_B_iso_or_equiv
   _atom_site_type_symbol
   Mn1      1.0    0.333334    0.666665    0.500000    Biso   1.000000 Mn
   Mn2      1.0    0.666666    0.333335    0.500000    Biso   1.000000 Mn
   P1       1.0    0.000999    0.001419    0.451326    Biso   1.000000 P
   P2       1.0    0.999001    0.998581    0.548674    Biso   1.000000 P
   S1       1.0    0.001485    0.680710    0.427682    Biso   1.000000 S
   S2       1.0    0.998515    0.319290    0.572318    Biso   1.000000 S
   S3       1.0    0.322880    0.323505    0.427681    Biso   1.000000 S
   S4       1.0    0.677120    0.676495    0.572319    Biso   1.000000 S
   S5       1.0    0.680086    0.002110    0.427682    Biso   1.000000 S
   S6       1.0    0.319914    0.997890    0.572318    Biso   1.000000 S
```

References

1   Cohen, A. J., Mori-Sánchez, P. & Yang, W. *Chemical reviews* **112**, 289-320, (2012).

2   Hafner, J. *Journal of computational chemistry* **29**, 2044-2078, (2008).

3   Kresse, G. & Joubert, D. *Phys. Rev. B* **59**, 1758, (1999).

4   Zhang, D., Hu, S., Sun, Y., Liu, X., Wang, H., Wang, H., Chen, Y. & Ni, Y. *ES Energy & Environment* **10**, 59-65, (2020).

5   Liu, X., Shao, X., Yang, B. & Zhao, M. *Nanoscale* **10**, 2108-2114, (2018).

6   Yu, J., Li, T., Nie, G., Zhang, B.-P. & Sun, Q. *Nanoscale* **11**, 10306-10313, (2019).

7   Li, W., Carrete, J., Katcho, N. A. & Mingo, N. *Computer Physics Communications* **185**, 1747-1758, (2014).

8   Ressouche, E., Loire, M., Simonet, V., Ballou, R., Stunault, A. & Wildes, A. *Phys. Rev. B* **82**, 100408, (2010).

9   Wildes, A. R., Roessli, B., Lebech, B. & Godfrey, K. W. *J. Phys.: Condens. Matter* **10**, 6417, (1998).

10   Ouvrard, G., Brec, R. & Rouxel, J. *Mater. Res. Bull.* **20**, 1181-1189, (1985).

11   Lee, S., Choi, K.-Y., Lee, S., Park, B. H. & Park, J.-G. *APL. Mater.* **4**, 086108, (2016).

12   Neal, S. N., Kim, H.-S., Smith, K. A., Haglund, A. V., Mandrus, D. G., Bechtel, H. A., Carr, G. L., Haule, K., Vanderbilt, D. & Musfeldt, J. L. *Phys. Rev. B* **100**, 075428, (2019).

13   Sun, Y.-J., Tan, Q.-H., Liu, X.-L., Gao, Y.-F. & Zhang, J. *J. Phys. Chem. Lett.* **10**, 3087-3093, (2019).

14   Mohamad Latiff, N., Rosli, N. F., Mayorga-Martinez, C. C., Szokolava, K., Sofer, Z., Fisher, A. C. & Pumera, M. *FlatChem* **18**, 100134, (2019).

15   Kargar, F., Coleman, E. A., Ghosh, S., Lee, J., Gomez, M. J., Liu, Y., Magana, A. S., Barani, Z., Mohammadzadeh, A., Debnath, B. *et al. ACS Nano* **14**, 2424-2435, (2020).

16   Alliati, I. M., Evans, R. F., Novoselov, K. S. & Santos, E. J. *arXiv preprint arXiv:2010.10466*, (2020).

17   Long, G., Henck, H., Gibertini, M., Dumcenco, D., Wang, Z., Taniguchi, T., Watanabe, K., Giannini, E. & Morpurgo, A. F. *Nano Lett.* **20**, 2452-2459, (2020).

18   Bai, W., Hu, Z., Xiao, C., Guo, J., Li, Z., Zou, Y., Liu, X., Zhao, J., Tong, W., Yan, W. *et al. J. Am. Chem. Soc.* **142**, 10849-10855, (2020).

19   Chu, H., Roh, C. J., Island, J. O., Li, C., Lee, S., Chen, J., Park, J.-G., Young, A. F., Lee, J. S. & Hsieh, D. *Phys. Rev. Lett.* **124**, 027601, (2020).

20   Wildes, A. R., Okamoto, S. & Xiao, D. *Phys. Rev. B* **103**, 024424, (2021).

21   Hicks, T. J., Keller, T. & Wildes, A. R. *J. Magn. Magn. Mater.* **474**, 512-516, (2019).

22   Chaudhuri, S., Kuo, C. N., Chen, Y. S., Lue, C. S. & Lin, J. G. *Phys. Rev. B* **106**, 094416, (2022).

23   Feringa, F., Vink, J. & van Wees, B. *arXiv preprint arXiv:2210.01418*, (2022).

24   Ni, Z., Zhang, H., Hopper, D. A., Haglund, A. V., Huang, N., Jariwala, D., Bassett, L. C., Mandrus, D. G., Mele, E. J., Kane, C. L. *et al. Phys. Rev. Lett.* **127**, 187201, (2021).

25   Long, G., Zhang, T., Cai, X., Hu, J., Cho, C.-w., Xu, S., Shen, J., Wu, Z., Han, T., Lin, J. *et al. ACS Nano* **11**, 11330-11336, (2017).

26   Babuka, T., Makowska-Janusik, M., Peschanskii, A. V., Glukhov, K. E., Gnatchenko, S. L. & Vysochanskii, Y. M. *Comp. Mater. Sci.* **177**, 109592, (2020).

27   Chittari, B. L., Park, Y., Lee, D., Han, M., MacDonald, A. H., Hwang, E. & Jung, J. *Phys. Rev. B* **94**, 184428, (2016).

28 Birowska, M., Faria Junior, P. E., Fabian, J. & Kunstmann, J. *Phys. Rev. B* **103**, L121108, (2021).

29 Alliati, I. M., Evans, R. F. L., Novoselov, K. S. & Santos, E. J. G. *NPJ Comput. Mater.* **8**, 3, (2022).

30 Xue, M., He, W., Gong, Q., Yi, M. & Guo, W. *Extreme Mechanics Letters*, 101900, (2022).

31 Kim, K., Lim, S. Y., Kim, J., Lee, J.-U., Lee, S., Kim, P., Park, K., Son, S., Park, C.-H., Park, J.-G. *et al. 2D Mater.* **6**, 041001, (2019).